Seismocardiograph Monitoring Using SMS Fiber Structure with PDMS Enclosure

Frans Rizal Agustiyanto[1,2], Agus M. Hatta[1*], Dhany Arifianto[1], Mahenda Radityo[1], Maulana Putra Santoso[1], Selfi Stendafity[1], and Budi Susetio Pikir[3]

[1] Department of Engineering Physics, Faculty of Industrial Technology and Systems Engineering, Institut Teknologi Sepuluh Nopember (ITS), 10 ITS str., Surabaya 60111, East Java, Indonesia

[2] Department of Physics Education, State Islamic University of Mahmud Yunus Batusangkar, 137 Sudirman General str., Tanah Datar 27212, West Sumatera, Indonesia

[3] Faculty of Medicine, Airlangga University, 47 Mayjen. Prof. Dr. Moestopo str., Surabaya 60132, East Java, Indonesia

e-mail: amh@its.ac.id

Abstract. This study presents a novel seismocardiography (SCG) monitoring system utilizing a singlemode-multimode-singlemode (SMS) fiber structure encased within a polydimethylsiloxane (PDMS) enclosure. The system employs a simple intensity-based interrogation method. Experimental characterization of the SMS fiber sensor demonstrated its sensitivity to vibrations, achieving an average calibration error of 1.63%. Validation against a gold-standard electrocardiogram (ECG) yielded an average error of 2.29%, representing a 1.27% accuracy improvement over existing fiber-optic SCG sensors (97.71% vs. 96.48%). This design offers a simplified and more robust alternative to current fiber-optic SCG sensors while maintaining high accuracy.

Keywords: fiber optic sensor; heart monitoring; polydhymetiloxane (PDMS); seismocardiography (SCG); singlemode-multimode-singlemode (SMS).

Paper #9167 received 24 Sept 2024; revised manuscript received 27 Dec 2024; accepted for publication 9 Jan 2025; published online 20 Mar 2025. doi: 10.18287/JBPE25.11.010303.

1 Introduction

Cardiovascular disease (CVD) remains a leading cause of global mortality, accounting for an estimated 17.9 million deaths in 2019, representing 32% of all deaths worldwide [1]. This burden disproportionately affects low- and middle-income countries, where over 75% of CVD deaths occur. Heart attacks and strokes are the primary contributors to this alarming mortality rate [1]. The rise in CVD prevalence is closely linked to modern lifestyles, emphasizing the urgent need for early prevention strategies to mitigate the associated risks [2].

Current clinical assessment of cardiovascular health relies on various diagnostic tools, including electrocardiography (ECG), magnetic resonance imaging (MRI), Computed Tomography (CT) scans, echocardiography, and nuclear myocardial perfusion scans. ECG, the most widely used method, records the heart's electrical activity, providing crucial insights into its function [3]. However, traditional ECG systems are often confined to hospital settings due to their size, complexity, and the need for specialized personnel.

To address these limitations, research has explored innovative solutions, such as wireless ECG sensors [4], smartphone-based ECG systems [5], and the application of convolutional neural networks (CNNs) for automated ECG analysis on wearable devices [6]. ECG data offers valuable information on various aspects of the cardiac cycle, including atrial and ventricular contraction and ventricular relaxation [7].

Seismocardiography (SCG) offers an alternative approach to cardiac monitoring. SCG measures mechanical vibrations generated by the heart's contraction and relaxation, providing insights into cardiac activity, including valve motion and ventricular filling time [8]. While SCG remains primarily a research tool with limited clinical application, its potential is being actively explored. Ongoing projects include the development of wearable SCG devices incorporating accelerometers and gyroscopes, with applications ranging from heart rate monitoring using machine learning algorithms [9] to the assessment of pre-ejection period (PEP) [10] and stroke volume (SV) in perioperative settings [11].

 doi: 10.18287/JBPE25.11.010303

Both SCG and ECG capture key physiological events like isovolumetric contraction, valve opening and closing, ejection, and heart filling [12]. Moreover, SCG has shown promise in predicting cardiac intervals such as left ventricular ejection time (LVET) and electromechanical systolic pre-ejection period (PEP) [8]. Consequently, ECG data can serve as a valuable reference for validating SCG signals from newly developed devices.

Limitations of accelerometer-based SCG and ECG during magnetic resonance imaging (MRI) necessitate alternative approaches for monitoring cardiac activity in this critical context [13]. Such monitoring is vital to ensure participant safety and mitigate anxiety-related complications [14]. Fiber optic sensors offer a promising solution due to their immunity to electromagnetic interference, potential for miniaturization, and cost-effective fabrication [14, 15].

Previous research has demonstrated the utility of fiber optic sensors for cardiac monitoring. Fiber Bragg Gratings (FBGs) have been employed to measure heart rates through vibrations transmitted to various surfaces [16], and also to assess respiration and heart rates simultaneously [17]. Singlemode-multimode-singlemode (SMS) fiber structures have emerged as an alternative to FBGs, offering advantages in fabrication simplicity, interrogation system complexity, and cost [18−20]. Notably, SMS fiber structures have been successfully utilized for apex cardiography [21] and integrated into smart beds for concurrent heart and respiration rate monitoring [22].

Prior research has demonstrated that encapsulating Fiber Bragg Gratings (FBGs) within a polydimethylsiloxane (PDMS) enclosure can substantially enhance optical fiber reflectivity, reaching up to 95.7% [14]. Building upon this concept, the present study investigates the application of a PDMS-enclosed SMS fiber structure sensor for SCG signal detection. The PDMS enclosure serves as a protective packaging for the sensor, aiming to maintain or improve SCG signal detection performance while providing crucial mechanical protection.

2 Materials and Methods

2.1 Fabrication and Calibration of SMS Structure Fiber Structure

The SMS fiber structure, depicted in Fig. 1, comprises a multimode fiber (MMF) section spliced between two single-mode fibers (SMFs). This SMS fiber construction utilizes a step-index MMF with a numerical aperture (NA) of 0.22 and MMF length of 45 mm as well as a singlemode optical fiber known as SMF28. The MMF section in the SMS fiber structure plays important role for the SMS fiber structure-based devices. The length of MMF section in the SMS fiber structure plays important role for the SMS fiber structure-based devices. A variation of MMF length can shift a spectral response [23] and a baseline intensity level [20] for a spectral wavelength measurement scheme using a broadband light source and an intensity measurement scheme at a fixed wavelength light source, respectively. This paper utilizes the intensity measurement scheme, which offers a simpler configuration compared to spectral wavelength measurement. While variations in the MMF length affect the baseline intensity for the SMS fiber structure, changes in the measurand (e.g., vibration, temperature, or strain) induce corresponding intensity variations. These variations, after suitable calibration, can be effectively employed for measurement or monitoring purposes.

Fig. 1 SMS structure fiber optic sensor configuration.

SMS fiber structures were fabricated using standard fiber optic equipment, including a fiber cleaver and a fusion splicer. To ensure precise MMF lengths in the SMS fiber structures, a digital caliper and a mechanical translation stage were employed during the cleaving and splicing process. This setup, as detailed in Ref. [23], allowed for precise MMF length control with an error margin of +/−0.5 mm. Several SMS structures with identical MMF specifications were fabricated and then encased in a protective polydimethylsiloxane (PDMS) enclosure.

Fig. 2 illustrates the experimental setup employed for vibration testing of the SMS fiber structure, a principle underpinning SCG monitoring. The sensor operates based on the acousto-optic effect: acoustic waves (generated by cardiac vibrations) induce strain in the fiber, altering its electrical permittivity through the photoelastic effect [24]. This strain, in turn, modifies the refractive index within the SMS fiber structure, leading to changes in the propagation constant and ultimately affecting the optical power output. Consequently, the heart’s vibrational pattern modulates the transmitted optical power, allowing for its detection and analysis [25].

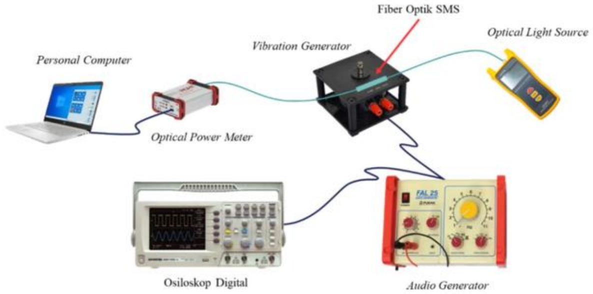

Fig. 2 PDMS Fiber-Optic Seismocardiograph calibration setup.

In the experimental setup, the SMS fiber structure is placed on a vibration generator (Pudak FAL29) connected to an oscilloscope (GW Instek GDS-1042) and a signal generator (Pudak FAL25). This configuration facilitates the acquisition of power fluctuation data and corresponding graphs resulting from vibrations in proximity to the optical fiber. Infrared light at a wavelength of 1550 nm and an optical power meter PM100USB from Thorlab was employed were utilized [21]. Fast Fourier Transform (FFT) is employed to convert the time-domain optical signal into the frequency domain, enabling the determination of its frequency components.

The SMS fiber structure is encased within a PDMS film, applied specifically to the multimode fiber (MMF) region. This encapsulation aims to mitigate the impact of environmental vibrations and disturbances that could potentially damage the delicate SMS fiber structure. The PDMS utilized in this study is in sheet form, with a thickness of 1 mm and dimensions of 80 mm (length) and 40 mm (width) [14]. Two PDMS sections are cut according to these dimensions, and the SMS fiber optic sensor is positioned between them. To investigate the influence of PDMS layer thickness on the sensor's output, varying thicknesses of 2 mm, 4 mm, and 6 mm are employed.

Calibration of the fabricated sensors, both unencapsulated and with varying enclosure thicknesses, was conducted using a vibration generator. Low-frequency vibrations within the range of 5−20 Hz, in 5 Hz increments, were applied. This frequency range was chosen to align with the typical low-frequency band of SCG signals, while avoiding higher frequencies prone to motion artifacts. The results of this calibration process are presented in Table 1.

As evident in Table 1, increasing enclosure thickness correlates with a higher average error. This observation can be attributed to the photoelastic effect: thicker enclosures dampen the vibrations reaching the SMS optical fiber, particularly within the sensitive MMF region, thereby reducing the sensor's response. Consequently, it is crucial to determine an optimal enclosure thickness that balances effective capture of cardiac vibrations with adequate protection for the optical fiber. In this study, a 2 mm thick enclosure was selected for subsequent data collection.

Table 1 Calibration results.

Reference frequency	Detected frequency			
	No enclosure	with 2 mm enclosure	with 4 mm enclosure	with 6 mm enclosure
5	5.021	5.1	5.14	5.22
10	10.198	10.2	10.44	10.31
15	15.237	15.19	14.89	15.37
20	20.4	20.29	20.22	20.4
Average error	1.01%	1.63%	2.25%	2.99%

3 Results

3.1 SCG Monitoring Using SMS Structure Fiber Optic Sensor with PDMS Enclosure

The SCG signal manifests as vibrations in the superficial layers of the body, particularly overlying the heart [8]. These vibrations induce strain in the MMF within the SMS fiber structure, leading to changes in multimode interference and, consequently, the output optical power. This photoelastic effect forms the basis of SCG signal transduction using the fiber optic sensor.

Fig. 3 illustrates the five potential sensor placements on the chest and thorax, each correlating to a specific cardiac region: position 1 (left ventricle), position 2 (left atrium), position 3 (right atrium), and positions 4 and 5 (right ventricle) [26]. For this study, the left ventricle (position 1) was chosen.

A healthy individual was selected as the participant for data collection. The sensor with PDMS enclosure was placed to the ventricle as in Fig. 4. A three-lead Heal Force Handheld Electrocardiogram ECG Monitor PC-80B with a single channel ECG was also placed to the participant allowing simultaneous SCG and ECG recordings.

Fig. 3 Seismocardiogram data collection positions.

Fig. 4 Data acquisition documentation of SMS fiber optic sensor with PDMS enclosure.

Figs. 5(a) and 5(b) show the measured optical power from the SMS fiber structure, and the ECG signal, respectively. It is noted that for SCG signal extraction, the optical power meter of PM100USB was set at a sampling frequency of 350 Hz. Raw data underwent pre-processing using a bandpass filter (0.5−25 Hz) to eliminate physiological motion artifacts. Subsequently, a smoothing technique was applied to segment the SCG signal into cardiac cycles, as detailed in Ref. [27]. To further reduce background noise arising from blood flow [28], an adjacent-average smoothing method was also employed. Fig. 5(c) presents the form of SCG signal.

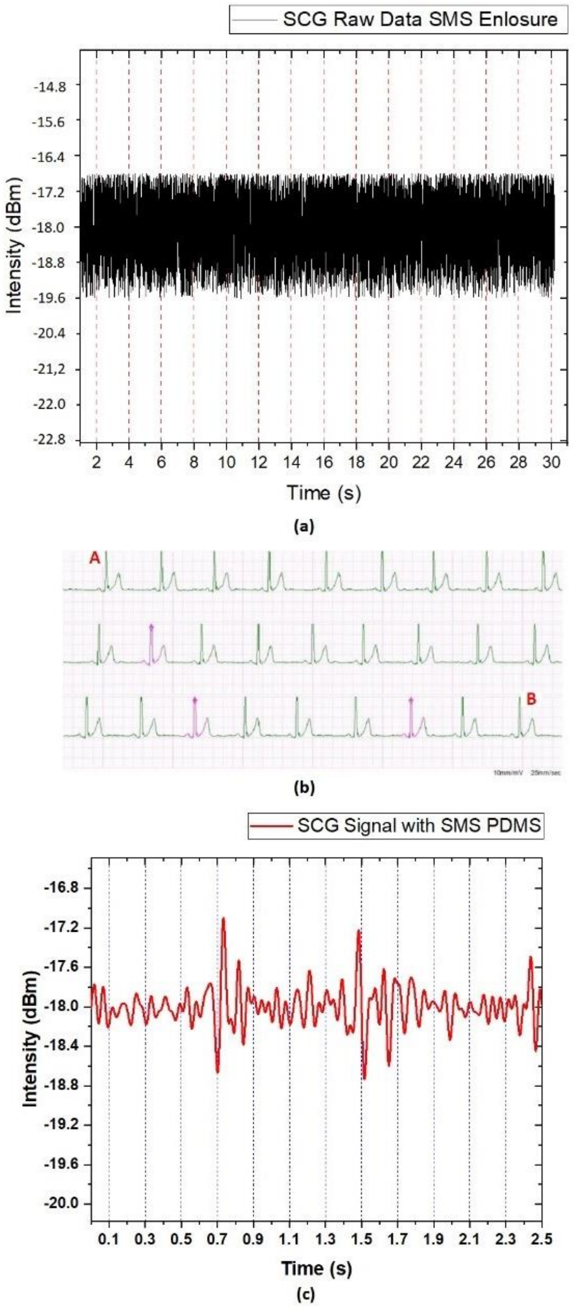

Fig. 5 (a) Raw data, (b) simultaneous ECG signal, and (c) filtered SCG signal.

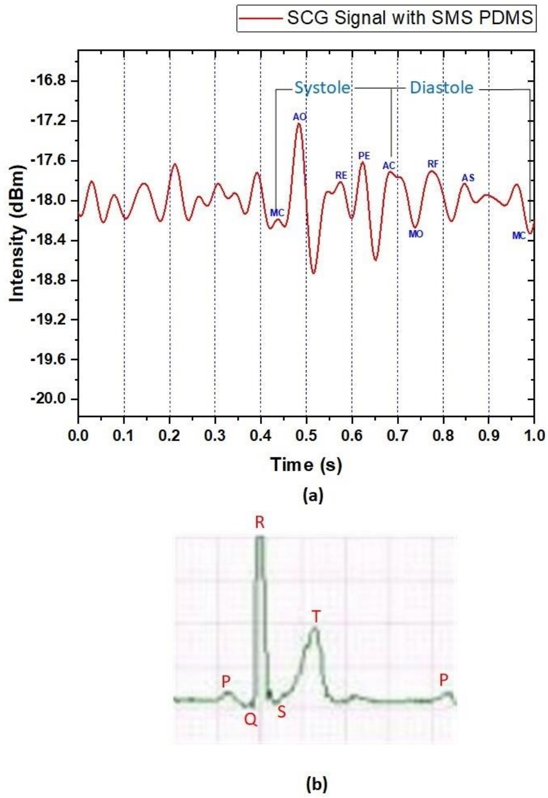

Fig. 6 Comparison of SCG and ECG signal, (a) one cycle of SCG signal with PDMS enclosure, (b) one cycle of simultaneous ECG signal.

The processed SCG signal was then compared to the ECG signal, as depicted in Fig. 6. Systolic and diastolic phases were identified from both signals: AO-AC and AC-MC peaks for SCG, and QRST and T-P intervals for ECG, respectively [8], as shown in Figs. 6(a) and 6(b). This work used a manual method to ascertain the location of each peak in both the SCG signals. By comparing it to a reference [13], the tallest peak was identified as the AO peak The other peaks (MC, RE, PE, AC, MO, RF, AS) were identified following the acquisition of the AO peak.

As a comparison to the measured SCG signal, an ECG recording using a three-lead Heal Force Handheld Electrocardiogram ECG Monitor PC-80B with a single channel ECG was conducted. The recorded ECG signal data were extracted to identify PQRST peaks and to determine T-P time interval as in Refs. [8, 13]. The ECG monitor can provide about 5 mm.mV ± 10% scale with a wave form sweeping speed of 20 mm/s ± 10%.

Tables 2 and 3 present a comparison of systolic and diastolic intervals derived from SCG and ECG signals, for the SMS fiber optic sensor without and with PDMS enclosure, respectively. Data validation involved 10 repetitions of SCG and ECG measurements. To assess the suitability of using the mean error value, the standard deviation of the overall error was calculated. For the unencapsulated sensor, the standard deviation was 0.0306, indicating acceptable homogeneity and justifying the use of the mean error [29]. The corresponding accuracy, derived from this mean error, was 96.48%.

Table 2 Comparison of systole and diastole periods (s) of SCG and ECG signals without PDMS enclosure.

No	ECG		SCG		Error	
	Systole	**Diastole**	**Systole**	**Diastole**	**Systole**	**Diastole**
1	0.49	0.72	0.55	0.69	9.86%	3.88%
2	0.49	0.50	0.52	0.48	6.12%	4.97%
3	0.33	0.67	0.32	0.67	1.54%	0.30%
4	0.50	0.72	0.52	0.72	3.58%	0.97%
5	0.32	0.63	0.31	0.63	1.89%	0.32%
6	0.41	0.52	0.42	0.52	0.97%	0.58%
7	0.33	0.47	0.30	0.49	9.37%	3.19%
8	0.40	0.46	0.40	0.47	0.99%	1.29%
9	0.46	0.53	0.44	0.49	4.32%	7.55%
10	0.41	0.72	0.41	0.78	1.48%	7.18%
		Average Error			3.52%	

Table 3 Comparison of systole and diastole periods (s) of SCG and ECG signals with PDMS enclosure.

No	ECG		SCG		Error	
	Systole	**Diastole**	**Systole**	**Diastole**	**Systole**	**Diastole**
1	0.34	0.45	0.37	0.48	8.89%	5.26%
2	0.38	0.57	0.38	0.58	1.05%	1.38%
3	0.33	0.65	0.30	0.63	9.43%	2.53%
4	0.36	0.64	0.35	0.66	2.29%	3.34%
5	0.34	0.64	0.34	0.64	1.17%	0.16%
6	0.34	0.68	0.33	0.68	2.99%	0.00%
7	0.44	0.62	0.44	0.61	0.23%	0.49%
8	0.33	0.58	0.33	0.58	0.61%	0.17%
9	0.33	0.64	0.34	0.65	4.13%	1.08%
10	0.46	0.60	0.46	0.60	0.43%	0.17%
		Average Error			2.29%	

For the PDMS-encapsulated sensor, the standard deviation of the overall error was 0.27729, again permitting the use of the mean error. The average error value, as shown in Table 3, demonstrates a marked improvement compared to the unencapsulated sensor, with a 53.7% reduction in error magnitude. The resulting accuracy for the encapsulated sensor was 97.71%.

The results highlight the efficacy of the PDMS enclosure in enhancing the accuracy and reliability of the SMS fiber optic sensor for SCG signal acquisition. The observed reduction in error magnitude and improved accuracy underscore the potential of this approach for developing robust and practical SCG monitoring systems.

To further evaluate the impact of the PDMS enclosure, we conducted a statistical analysis comparing measurements with and without the enclosure (Tables 2 and 3). Our analysis revealed no statistically significant difference between the two datasets for both systolic and diastolic measurements (p-values of 0.536 and 0.173, respectively). These p-values exceed the 0.05 significance level, indicating that observed variations are likely due to random fluctuations and the limited sample size. While a larger study might yield more definitive conclusions, our findings suggest that the PDMS enclosure does not negatively affect sensor performance. This observation aligns with previous research [30] where PDMS was successfully employed in flexible mechanical sensors. PDMS, with its Poisson's ratio near 0.5, exhibits incompressibility, making it highly sensitive to even small deformations, which is beneficial for sensor applications.

4 Conclusions

This study investigated the feasibility of a novel SCG monitoring system utilizing a SMS fiber structure encased in a protective PDMS enclosure. Positioned on the anterior thorax to capture cardiac vibrations, the sensor's optical power output was processed to generate the SCG signal. Calibration using vibration and audio signals (5−20 Hz) demonstrated high accuracy, with an average error of 1.63%. Validation against a gold-standard electrocardiogram (ECG) confirmed the sensor's reliability, achieving an average error of 2.29% and an overall accuracy of 97.71%. This represents a 1.27% improvement compared to existing fiber-optic SCG sensors. Statistical analysis further confirmed that the PDMS enclosure did not negatively impact sensor performance while providing essential mechanical protection. This novel SCG system offers a promising pathway for developing reliable and cost-effective cardiac monitoring solutions.

Acknowledgments

This work was supported by "Hibah Penelitan Doktoral" from Ministry of Education and Research Technology, Indonesia.

Funding

This research received funding from the "Hibah Penelitan Doktoral" under contract number 1689/PKS/ITS/2024 from the Ministry of Education and Research Technology, Indonesia.

Data Availability Statement

The data presented in this study are available on request from the corresponding author.

Disclosures

The authors declare that they have no known competing financial interests or personal relationships that could have appeared to influence the work reported in this paper.

References

1. World Health Organization, "World health statistics 2023: monitoring health for the SDGs, Sustainable Development Goals," Geneva, 19 May 2023 (accessed 22 June 2023).
2. M. Y. Desai, S. Windecker, P. Lancellotti, J. J. Bax, B. P. Griffin, O. Cahlon, and D. R. Johnston, "Prevention, diagnosis, and management of radiation-associated cardiac disease," Journal of the American College of Cardiology 74(7), 905–927 (2019).
3. P. K. Jain, A. K. Tiwari, "Heart monitoring systems—A review," Computers in Biology and Medicine 54, 1–13 (2014).
4. S. Majumder, L. Chen, O. Marinov, C.-H. Chen, T. Mondal, and M. J. Deen, "Noncontact wearable wireless ecg systems for long-term monitoring," IEEE Reviews in Biomedical Engineering 11, 306–321 (2018).
5. H. T. Haverkamp, S. O. Fosse, and P. Schuster, "Accuracy and usability of single-lead ECG from smartphones - A clinical study," Indian Pacing and Electrophysiology Journal 19(4), 145–149 (2019).
6. L. Meng, K. Ge, Y. Song, D. Yang, and Z. Lin, "Long-term wearable electrocardiogram signal monitoring and analysis based on convolutional neural network," IEEE Transactions on Instrumentation and Measurement 70, 1–11 (2021).
7. B. Ngai, K. Tavakolian, A. Akhbardeh, A. P. Blaber, B. Kaminska, and A. Noordergraaf, "Comparative analysis of seismocardiogram waves with the ultra-low frequency ballistocardiogram," Annual International Conference of the IEEE Engineering in Medicine and Biology Society, 2851–2854 (2009).
8. A. Taebi, B. E. Solar, A. J. Bomar, R. H. Sandler, and H. A. Mansy, "Recent advances in seismocardiography," Vibration 2(1), 64–86 (2019).
9. O. T. Inan, M. Baran Pouyan, A. Q. Javaid, S. Dowling, M. Etemadi, A. Dorier, J. A. Heller, A. O. Bicen, S. Roy, T. De Marco, and L. Klein, "Novel wearable seismocardiography and machine learning algorithms can assess clinical status of heart failure patients," Circ: Heart Failure 11(1), e004313 (2018).
10. M. M. H. Shandhi, B. Semiz, S. Hersek, N. Goller, F. Ayazi, and O. T. Inan, "Performance analysis of gyroscope and accelerometer sensors for seismocardiography-based wearable pre-ejection period estimation," IEEE Journal of Biomedical and Health Informatics 23(6), 2365–2374 (2019).
11. B. Semiz, A. M. Carek, J. C. Johnson, S. Ahmad, J. A. Heller, F. G. Vicente, S. Caron, C. W. Hogue, M. Etemadi, and O. T. Inan, "Non-invasive wearable patch utilizing seismocardiography for peri-operative use in surgical patients," IEEE Journal of Biomedical and Health Informatics 25(5), 1572–1582 (2021).
12. P. K. Sahoo, H. K. Thakkar, W.-Y. Lin, P.-C. Chang, and M.-Y. Lee, "On the design of an efficient cardiac health monitoring system through combined analysis of ecg and scg signals," Sensors 18(2), 379 (2018).

13. J. Kolarik, R. Kahankova, J. Brablik, and R. Martinek, "Comparison of SCG and ECG based cardiac activity monitoring in laboratory conditions," IFAC-PapersOnLine 52(27), 550–555 (2019).
14. J. Nedoma, M. Fajkus, P. Siska, R. Martinek, and V. Vasinek, "Non-invasive fiber optic probe encapsulated into polydimethylsiloxane for measuring respiratory and heart rate of the human body," Advances in Electrical and Electronic Engineering 15(1), 93–100 (2017).
15. C. Perezcampos Mayoral, J. Gutiérrez Gutiérrez, J. L. Cano Pérez, M. Vargas Treviño, I. B. Gallegos Velasco, P. A. Hernández Cruz, R. Torres Rosas, L. Tepech Carrillo, J. Arnaud Ríos, E. L. Apreza, and R. Rojas Laguna, "Fiber optic sensors for vital signs monitoring. a review of its practicality in the health field," Biosensors 11(2), 58 (2021).
16. Y. S. Yaras, O. Kocaturk, and F. L. Degertekin, "FBG based electric field sensor for MRI safety," in Proceedings of Optical Sensors and Sensing Congress, STu4D.7 (2020).
17. C. Tavares, C. Leitão, D. Lo Presti, M. F. Domingues, N. Alberto, H. Silva, and P. Antunes, "Respiratory and heart rate monitoring using an FBG 3D-printed wearable system," Biomedical Optics Express 13(4), 2299 (2022).
18. N. Irawati, A. M. Hatta, Y. G. Y. Yhuwana, and Sekartedjo, "Heart rate monitoring sensor based on singlemode-multimode-singlemode fiber," Photonic Sensors 10(2), 186–193 (2020).
19. Q. Wu, A. M. Hatta, P. Wang, Y. Semenova, and G. Farrell, "Use of a bent single sms fiber structure for simultaneous measurement of displacement and temperature sensing," IEEE Photonics Technology Letters 23(2), 130–132 (2011).
20. A. M. Hatta, Y. Semenova, Q. Wu, and G. Farrell, "Strain sensor based on a pair of single-mode-multimode-single-mode fiber structures in a ratiometric power measurement scheme," Applied Optics 49(3), 536–541 (2010).
21. F. R. Agustiyanto, A. M. Hatta, D. Arifianto, and B. S. Pikir, "Use of a singlemode multimode singlemode fiber structure for apex cardiography monitoring," in Fourth International Seminar on Photonics, Optics, and Its Applications, Proceedings of SPIE 117892, 117890E (2021).
22. N. R. Amalia, A. M. Hatta, S. Koentjoro, A. M. T. Nasution, and I. Puspita, "Fiber sensor for simultaneous measurement of heart and breath rate on smartbed," in IEEE 8th International Conference on Photonics, IEEE, 68–69 (2020).
23. A. M. Hatta, G. Farrell, Q. Wang, G. Rajan, P. Wang, and Y. Semenova, "Ratiometric wavelength monitor based on singlemode-multimode-singlemode fiber structure," Micro & Optical Tech Letters 50(12), 3036–3039 (2008).
24. A. Yariv, P. Yeh, "Optical waves in crystal propagation and control of laser radiation," (1983).
25. Y. Zhao, X. Li, F. Meng, and Z. Zhao, "A vibration-sensing system based on SMS fiber structure," Sensors and Actuators A: Physical 214, 163–167 (2014).
26. T. Allsop, G. Lloyd, R. S. Bhamber, L. Hadzievski, M. Halliday, D. J. Webb, and I. Bennion, "Cardiac-induced localized thoracic motion detected by a fiber optic sensing scheme," Journal of Biomedical Optics 19(11), 117006 (2014).
27. P. K. Jain, A. K. Tiwari, "An algorithm for automatic segmentation of heart sound signal acquired using seismocardiography," in 2016 International Conference on Systems in Medicine and Biology, 157–161 (2016).
28. S. Koyama, T. Hayase, S. Miyauchi, A. Shirai, S. Chino, Y. Haseda, and H. Ishizawa, "Influence on measurement signal by pressure and viscosity changes of fluid and installation Condition of FBG sensor using blood flow simulation model," IEEE Sensors Journal 19(24), 11946–11954 (2019).
29. S. El Omda, S. R. Sergent, "Standard deviation," StatPearls Publishing, Treasure Island (FL) (2021).
30. Q. She, P. Wu, W. Lin, Y. Huang, F. Wang, and Z. Ye, "Design of flexible mechanical sensor based on PDMS grating," Advanced Fiber Laser Conference 12595, 560–566 (2023).